British Journal of Nutrition (2020), 123, 1117–1126

doi:10.1017/S0007114520000549

British Journal of Nutrition

Tricarboxylic acid cycle dehydrogenases inhibition by naringenin: experimental and molecular modelling evidence

Pauline Maciel August[1], Mateus Grings[1], Marcelo Sartori Grunwald[1], Geancarlo Zanatta[2], Vinícius Stone[1], Patricia Idalina de Lemos Rodrigues[3], Daniela Pereira Stocher[3], José Cláudio Fonseca Moreira[1,3], Guilhian Leipnitz[1,3] and Cristiane Matté[1,3,4]*

[1]*Programa de Pós-graduação em Ciências Biológicas: Bioquímica, ICBS, Universidade Federal do Rio Grande do Sul, Porto Alegre, RS, Brazil*
[2]*Departamento de Física, Universidade Federal do Ceará, Fortaleza, CE, Brazil*
[3]*Departamento de Bioquímica, Instituto de Ciências Básicas da Saúde, Universidade Federal do Rio Grande do Sul, Porto Alegre, RS, Brazil*
[4]*Programa de Pós-graduação em Ciências Biológicas: Fisiologia, ICBS, Universidade Federal do Rio Grande do Sul, Porto Alegre, RS, Brazil*

(Submitted 24 July 2019 – Final revision received 14 January 2020 – Accepted 6 February 2020 – First published online 20 February 2020)

Abstract

The study of polyphenols' effects on health has been gaining attention lately. In addition to reacting with important enzymes, altering the cell metabolism, these substances can present either positive or negative metabolic alterations depending on their consumption levels. Naringenin, a citrus flavonoid, already presents diverse metabolic effects. The objective of this work was to evaluate the effect of maternal naringenin supplementation during pregnancy on the tricarboxylic acid cycle activity in offspring's cerebellum. Adult female Wistar rats were divided into two groups: (1) vehicle (1 ml/kg by oral administration (p.o.)) or (2) naringenin (50 mg/kg p.o.). The offspring were euthanised at 7th day of life, and the cerebellum was dissected to analyse citrate synthase, isocitrate dehydrogenase (IDH), α-ketoglutarate dehydrogenase (α-KGDH) and malate dehydrogenase (MDH) activities. Molecular docking used SwissDock web server and FORECASTER Suite, and the proposed binding pose image was created on UCSF Chimera. Data were analysed by Student's *t* test. Naringenin supplementation during pregnancy significantly inhibited IDH, α-KGDH and MDH activities in offspring's cerebellum. A similar reduction was observed *in vitro*, using purified α-KGDH and MDH, subjected to pre-incubation with naringenin. Docking simulations demonstrated that naringenin possibly interacts with dehydrogenases in the substrate and cofactor binding sites, inhibiting their function. Naringenin administration during pregnancy may affect cerebellar development and must be evaluated with caution by pregnant women and their physicians.

Key words: **Flavonoids: Supplementation: Pregnancy: Metabolic programming: Offspring**

As a part of a healthier agenda, antioxidant intake has increased in society. Supplementation with polyphenol family members, as flavonoids found in plants[38,55], has become common, and its frequent consumption is associated with decreased risk for chronic diseases, such as diabetes and CVD[60,82,83], also affecting energy metabolism[8,42]. The effect of polyphenols on glucose metabolism has already been demonstrated by several processes, from the inhibition of the key enzymes in dietary carbohydrate digestion, α-amylase and α-glucosidase, to increased insulin sensitivity and hepatic glucokinase mRNA expression in mice[44].

Pregnancy is a key developmental period whereby aberrant fetal programming due to a suboptimal maternal environment can increase the risk for the development of a range of disease across the life course[4,5,24,29]. Early exposure to unsettled milieu, such as maternal obesity, infection or stress, leads to higher TAG levels and impaired glucose homeostasis in the offspring, resulting in early obesity and cardiac hypertrophy[23,73]. In addition, a stressful maternal environment increases the risk for neurodevelopmental disorders including schizophrenia, depression and autism[12,54,81]. When supplemented during pregnancy, flavonoids prevented stress-induced disorders in mouse pups[75] and reduced DNA damage in adult offspring[77].

Naringenin, the aglycone form of naringin, is a flavanone commonly found in citrus fruits such as tangerines, grapefruits and

Abbreviations: α-KGDH, α-ketoglutarate dehydrogenase; IDH, isocitrate dehydrogenase; MDH, malate dehydrogenase; TCA, tricarboxylic acid.

* **Corresponding author:** Cristiane Matté, fax +55 51 3308 5535, email matte@ufrgs.br

lemons. It has shown antioxidant capacity and protection against oxidative stress and cognitive impairment[41,79]. The use and safety of polyphenols during pregnancy remain a subject of debate, since increased consumption of polyphenols during the third trimester of pregnancy was related to negative dynamics of fetal ductus arteriosus[87,88], and the maternal restriction of polyphenol intake blockaded the effect[90], making polyphenol consumption during pregnancy a cause for concern[28,47]. These findings highlight the importance of experimental animal models to examine the effects of polyphenol supplementation in offspring, principally taking into consideration the critical developmental period and possible longer term outcomes.

In view of the lack of studies showing the effect of redox active substances intake during pregnancy, the objective of this study was to evaluate whether the naringenin supplementation during pregnancy might interfere on tricarboxylic acid (TCA) cycle activity in the cerebellum of rat offspring. Once we verified the significant inhibitory effect of naringenin on dehydrogenases activities, we investigated the mechanism involved using the bioinformatics approach.

Materials and methods

Animals and reagents

Twenty-four adult female (90 d of age) and twelve adult male Wistar rats (60 d of age), with an average weight of 220 and 250 g, respectively, were obtained from the Central Animal House of Departamento de Bioquímica, Instituto de Ciências Básicas da Saúde, Universidade Federal do Rio Grande do Sul, Porto Alegre, RS, Brazil. Animals were maintained in a 12 h light–12 h dark cycle in an air-conditioned constant temperature (22 (SD 1)°C) colony room. The animals had free access to water and a 20 % (w/w) protein commercial chow.

The experiments were approved by the local Ethics Commission (Comissão de Ética no Uso de Animais - Universidade Federal do Rio Grande do Sul) under the number 26542, and followed national animal rights regulations (Law 11.794/2008), the National Institutes of Health Guide for the Care and Use of Laboratory Animals (NIH publication no. 80–23, revised 1996), directive 2010/63/EU, as well as the Animal Research: Reporting of In Vivo Experiments Guidelines for Reporting Animal Research. We further attest that all efforts were made to minimise the number of animals used and their suffering.

All chemicals were obtained from Sigma Chemical Co.

In vivo *experimental design*. Female rats were randomly divided into two groups (n 8 each): (1) control, receiving vehicle (1 ml/kg by oral administration (p.o.)) and (2) naringenin (50 mg/kg p.o.). The method of oral gavage was introduced to the animals 1 week prior to pregnancy to habituate them to the procedure. The administration of naringenin and/or vehicle was started only after mating (when animals were kept one male per two females per cage), during the morning, first with the administration of the vehicle in the control group and after the naringenin administration in the treated group. Pregnancy was diagnosed by the presence of a vaginal plug. From the 20th day after the onset of pregnancy, we isolated the pregnant dams (one per cage) and the rats were observed twice a day (at 09.00 hours and 18.00 hours), to verify the litter's birth. The day corresponding to the offspring's birth is defined as postnatal day 0.

The offspring were left with the mother until postnatal day 7 when both mother and offspring were euthanised by decapitation without anaesthesia. Cerebella was dissected and stored at −80°C until the completion of the biochemical assays. One pup from each litter was used for each assay, in order to eliminate the litter effect.

Naringenin supplementation. Naringenin (50 mg/kg) was suspended in sunflower oil (1 ml/kg), which was used as vehicle, and administered by gavage 5 d/week (Monday to Friday) for the 3 weeks of pregnancy to treated rats. The dose was defined according to its neuroprotective action[62,64] and did not interfere on pregnancy rate, gestational weight gain, litter size or weight at birth, as shown previously[3].

Biochemical assays

Sample preparation. Mitochondrial fraction was isolated from the offspring's cerebellum as described by Rosenthal *et al.*[63], with slight modifications. Animals were euthanised by decapitation, had their cerebellum rapidly removed and put into ice-cold isolation buffer containing 225 mM mannitol, 75 mM sucrose, 1 mM EGTA, 0·1 % bovine serum albumin (free of fatty acids) and 10 mM HEPES, pH 7·2. The cerebellum was homogenised 1:10. The homogenate was centrifuged for 3 min at 2000 ***g***. After centrifugation, the supernatant was again centrifuged for 8 min at 12 000 ***g***. The pellet was suspended in isolation buffer containing 4 µl of 10 % digitonin and centrifuged for 10 min at 12 000 ***g***. The supernatant was discarded, and the final pellet was gently washed and suspended in isolation buffer devoid of EGTA, at an approximate protein concentration of 2·5 mg/ml.

Determination of citrate synthase activity. Citrate synthase was measured according to Srere[69], by determining 5,5′-dithiobis-(2-nitrobenzoic acid) (DTNB) reduction at $\lambda = 412$ nm, and calculated as nmol TNB/min per mg protein. The reaction mixture contained 5 mM potassium phosphate buffer, pH 7·4, 300 mM sucrose, 1 mM EGTA, 0·1 % bovine serum albumin, 5 mM 3-(N-morpholino) propanesulfonic acid (MOPS), 0·1 % Triton X-100, 0·1 mM DTNB, 0·1 mM acetyl-CoA and 0·2 mM oxaloacetate.

Determination of isocitrate dehydrogenase activity. Isocitrate dehydrogenase (IDH) was evaluated according to Plaut[59], by following NAD^+ reduction fluorimetrically at excitation and emission wavelengths of 340 and 466 nm, respectively. The reaction mixture contained mitochondrial preparations, 33 mM Tris-HCl buffer, pH 7·4, 10 µM rotenone, 1·2 mM $MnCl_2$, 0·67 mM ADP, 0·1 % Triton X-100, 0·6 mM NAD^+ and 5 mM isocitrate. IDH activity was calculated and expressed as nmol $NADH.H^+$/min per mg protein.

Determination of α-ketoglutarate dehydrogenase activity. The activity of α-ketoglutarate dehydrogenase (α-KGDH) complex was evaluated according to Lai & Cooper[46] and Tretter &

British Journal of Nutrition

Adam-Vizi[76] with some modifications. The incubation medium contained mitochondrial preparations, 1 mM $MgCl_2$, 0·2 mM thiamine pyrophosphate, 0·4 mM ADP, 10 μM rotenone, 0·2 mM EGTA, 0·12 mM coenzyme A-SH, 1 mM α-ketoglutarate, 2 mM NAD^+, 0·1 % Triton X-100 and 50 mM potassium phosphate, pH 7·4. The reduction of NAD^+ was recorded at excitation and emission wavelengths of 366 and 450 nm, respectively. α-KGDH activity was calculated and expressed as nmol $NADH.H^+$/min per mg protein.

Determination of malate dehydrogenase activity. Malate dehydrogenase (MDH) activity was measured according to Kitto[45]. The incubation medium consisted of mitochondrial preparations, 10 μM rotenone, 0·1 % Triton X-100, 0·14 mM $NADH.H^+$, 0·3 mM oxaloacetate and 50 mM potassium phosphate, pH 7·4. MDH activity was determined following the reduction of $NADH.H^+$ fluorescence at excitation and emission wavelengths of 366 and 450 nm, respectively. MDH activity was calculated and expressed as μmol $NADH.H^+$/min per mg protein.

In vitro *experimental design*

Naringenin (60 ng/ml) was dissolved in ethanol and added into the incubation medium for the determination of the direct effect on dehydrogenases (α-KGDH and MDH) activities. The α-KGDH complex was evaluated according to Lai and Cooper[46] and Tretter & Adam-Vizi[76], while MDH activity was measured according to Kitto[45], as described above. Naringenin concentration was used due to the naringenin level demonstrated in blood, minutes after ingestion[49,72].

Protein determination

Protein concentration was measured by the method of Lowry *et al.*[48] using bovine serum albumin as standard.

Statistical analysis

Data were analysed by Student's *t* test, using GraphPad Prism 6.0 software. Data were considered statistically significant when $P < 0{\cdot}05$. Considering $\alpha = 0{\cdot}05$ and $\beta = 0{\cdot}20$ (using the biostatistics method[10]), we used a sample size of eight in animal biochemical parameters.

Molecular docking, structural analyses and interaction energy calculation

FORECASTER suite analysis. The bacterial protein structures in distinct conformations obtained from the Research Collaboratory for Structural Bioinformatics Protein Data Bank (http://www.rcsb.org/pdb/home/home.do) were employed in the molecular docking calculations and are listed as the following:

(a) Structures representing IDH: 1J1W, in complex with NADP[86], 2QFV, in complex with NADP[58], 2QFW, in complex with ICT[58], 3MBC, in complex with NADP[68], 1AI3, in complex with NDO[50], 1CW1, in complex with ICT[14], 1CW7, in complex with ICT[14], 1ITW, in complex with ICT[85], 4AJ3, in complex with NADP and ICT[27] and 4AJ8, in complex with NADPH and 1K9[11].
(b) Structures representing MDH: 1BMD, in complex with NAD^+[40], 2CMD, in complex with CIT[31], 1B8U, in complex with NAD^+[43], 1EMD, in complex with NAD^+ and CIT[30], 1Y7T, in complex with NADPH[74], 1BDM, in complex with NAD^+[40] and 1IE3, in complex with NAD^+ and PYR[6].
(c) Structures representing SDH: 1YQ3, in complex with FAD and UBQ[33], 1NEK, in complex with FAD[84], 1NEN, in complex with dinitrophenol-17 inhibitor ubiquinone binding site[84], 4YXD, in complex with FTN[35] and 1ZOY, in complex with FAD and UBQ1[71].

Naringenin structure was retrieved from the ZINC database (ZINC00001785) in .sdf format.

Molecular docking. Docking calculations were performed on the FORECASTER Suite, including the FITTED docking software, from Molecular Forecaster Inc. It uses a more accurate protein model and is based on a pharmacophore-oriented docking method combined with a genetic algorithm based-docking approach. Proteins, ligands and potential bridging water molecules are described as genes, and a mixed Lamarckian/Darwinian evolution optimises the whole complex. In this step, the ligands present in the crystal structures were identified by the software, creating a binding site. Ligands were then tested to bind in these specific locations, and the score of the docking poses was calculated and compared. The proposed binding to the active pocket of the enzymes was determined as the best-ranked scoring function, representing the conformational structures with the most favourable free binding energy (ΔG). Structural analyses and the proposed binding pose images were created on BIOVIA Discovery Studio 3.5.

Autodock4 analysis. The protein structures of human MDH in distinct conformations obtained from Research Collaboratory for Structural Bioinformatics Protein Data Bank server (www.rcsb.org)[7] were employed in the molecular docking calculations and are listed as the following: 4WLN, in apo state[19], 4WLV, in complex with NAD^+[20], 4WLF, in complex with L-malate[21] and 4WLU, in complex with NAD^+ and L-malate[22]. Naringenin molecule was retrieved from the ZINC database[36].

The crystals' asymmetric unit cell contains four subunits (A, B, C and D) exhibiting no significant differences. We arbitrarily chose subunit A to prepare the docking input. The preparation of the molecular structure of naringenin and the validation of protonation state at physiological pH were accomplished using the Marvin Sketch code version 5.5.0.1 (Marvin Beans Suite – ChemAxon). The protonation state of MDH was adjusted according to results obtained from the PROPKA code form PDB2PQR Web Server 2.1.1 (http://www.poissonboltzmann.org/docs/structures-ready)[17,18].

Molecular docking. Molecular docking was performed using Autodock4[34,53] after protocol validation through the redocking of NAD^+ and malate, as described elsewhere[32,51]. Docking procedure was repeated twenty times, resulting in 400 poses (twenty poses per output). The procedure was set to use a

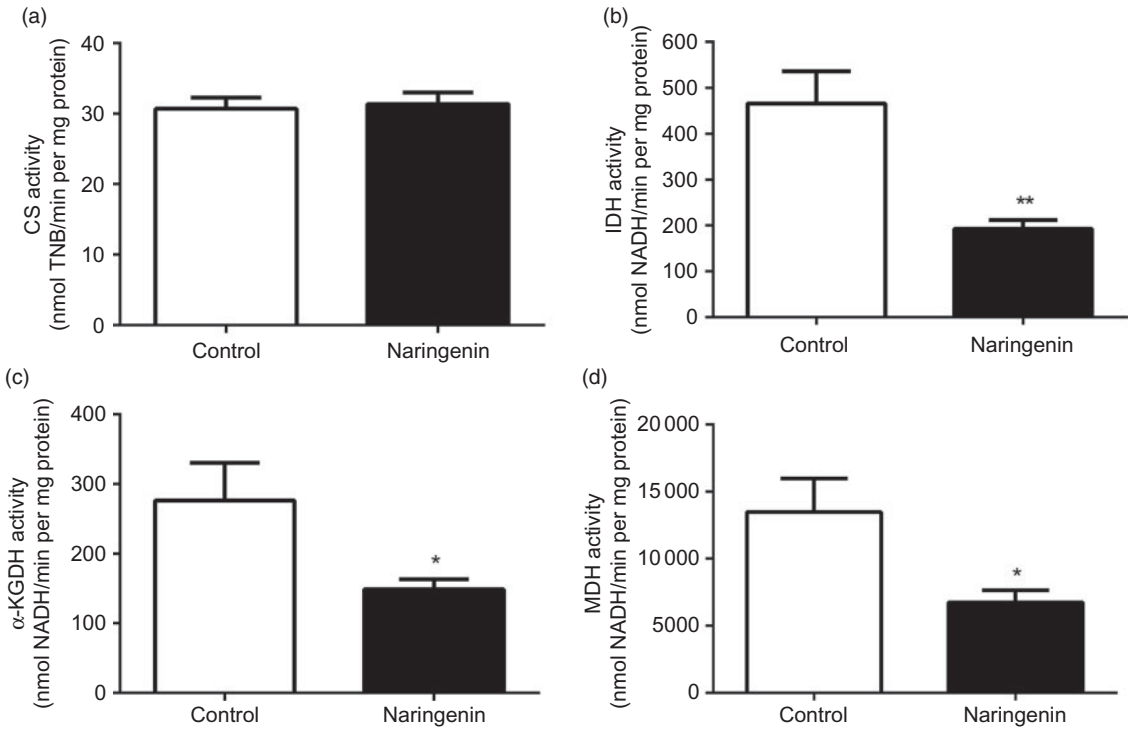

Fig. 1. Effect of naringenin supplementation during pregnancy on (a) citrate synthase (CS), (b) isocitrate dehydrogenase (IDH), (c) α-ketoglutarate dehydrogenase (α-KGDH) and (d) malate dehydrogenase (MDH) activities in offspring's cerebellum. Results are mean values and standard errors for *n* 8 performed in triplicate. Data were analysed by Student's *t* test. * $P < 0{\cdot}05$; ** $P < 0{\cdot}01$.

Lamarckian genetic algorithm[52], a genetic algorithm with 25 000 000 energy evaluations per run, population size set to 150 and a maximum of 27 000 generations per run. In the end, resulting poses were clustered using a root-mean-square deviation (RMSD) tolerance of 2·0 Å^2 using Autodock Tools[53,65].

Naringenin was used for the docking into the MDH binding pocket within a rigid-protein protocol. Among the clusters formed under a RMSD tolerance of 2·0 Å^2, the first pose of the clusters with better binding energy (or with more poses) was analysed to choose the best representative pose. Structures were built using Discovery Studio 4.1 Client and figures prepared using PyMOL 1.3[67]. Simulations took into consideration the complexity of the catalytic mechanism involving MDH, which involves conformational changes in the binding cleft due to the binding of NAD followed by L-malate.

Results

Naringenin administration during pregnancy inhibited Krebs cycle dehydrogenases activities in the offspring's cerebellum

Fig. 1 shows the activities of citrate synthase, IDH, α-KGDH and MDH measured in postnatal day 7 pups' cerebellum, subjected to maternal naringenin administration during pregnancy. Even though citrate synthase was not affected ($t(12) = 0{\cdot}2986$; $P = 0{\cdot}7703$) (Fig. 2(a)), the naringenin supplementation during pregnancy was able to decrease IDH ($t(10) = 4{\cdot}388$;

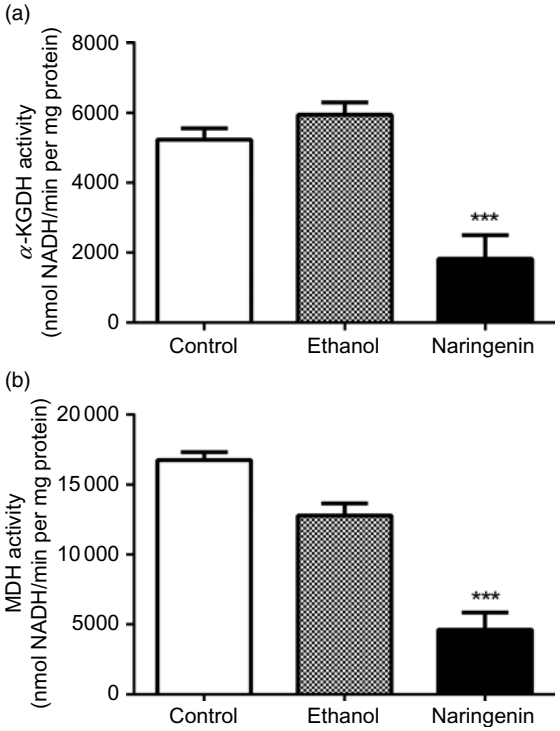

Fig. 2. *In vitro* effect of naringenin on (a) α-ketoglutarate dehydrogenase (KGDH) and (b) malate dehydrogenase (MDH) activities. Results are mean values and standard errors for *n* 1 performed in triplicate. Data were analysed by one-way ANOVA followed by Tukey's test. ***$P < 0{\cdot}001$.

$P = 0{\cdot}0014$), α-KGDH ($t(11) = 2{\cdot}441$; $P = 0{\cdot}0327$) and MDH activities ($t(12) = 2{\cdot}532$; $P = 0{\cdot}0263$) evaluated in pups' cerebellum (Fig. 2(b), (c), and (d); respectively).

Naringenin directly inhibited purified Krebs cycle dehydrogenases

Considering that naringenin supplementation inhibited all the Krebs cycle dehydrogenases *in vivo*, we wondered whether this polyphenol could interact directly with these enzymes. In order to clarify this aspect, we evaluated the effect of naringenin on commercially available purified enzymes that use NAD^+ as a coenzyme. Fig. 2 shows the activities of purified α-KGDH and MDH measured under the *in vitro* effect of naringenin (60 ng/ml) and its vehicle, ethanol. *In vitro* incubation with naringenin inhibited both dehydrogenases, KGDH ($F_{2,15} = 48{\cdot}69$; $P < 0{\cdot}0001$) and MDH activity ($F_{2,15} = 43{\cdot}53$; $P < 0{\cdot}0001$), as observed in Fig. 2(a) and (b), respectively.

Naringenin possibly bind to different sites on enzymes structures

To understand the relationship of naringenin and the enzymes tested *in vivo* and *in vitro*, and to simulate binding between the enzymes and the flavonoid, we used two different assessment methods, being one of them FORECASTER Suite, and the other Autodock4. By doing this, we could evaluate the possible interaction. The molecular docking method applied on FORECASTER Suite identified the co-crystallised ligands in the enzymes structures, and their respective binding site was extracted and later utilised in a targeted docking with the selected compound. When the protein structure had more than one ligand complexed, the different binding sites were tested on separated docking runs, for example, the interaction was tested on the sites for cofactors and for substrates, making possible to compare the preferred sites on which naringenin could possibly bind. The results in terms of binding free energy (ΔG) value for the binding modes between naringenin, IDH and MDH are listed in Tables 1 and 2, respectively.

Table 1. Summary of molecular docking experiments of naringenin and bacterial isocitrate dehydrogenase

Target name	PDB code	Binding free energy (kcal/mol)*
Isocitrate dehydrogenase 1K9 complexed	4JA8	−1·09
Isocitrate dehydrogenase ICT complexed	1CW1	−32·73
Isocitrate dehydrogenase ICT complexed	1CW7	−21·22
Isocitrate dehydrogenase ICT complexed	1ITW	−40·95
Isocitrate dehydrogenase ICT complexed	4AJ3	−32·80
Isocitrate dehydrogenase ICT complexed	2QFW	−33·69
Isocitrate dehydrogenase NADP complexed	1J1W	−47·40
Isocitrate dehydrogenase NADP complexed	2QFV	−35·33
Isocitrate dehydrogenase NADPH complexed	4JA8	−33·51
Isocitrate dehydrogenase NADP complexed	3MBC	−36·83
Isocitrate dehydrogenase NADP complexed	4AJ3	−33·39
Isocitrate dehydrogenase NDO complexed	1AI3	−27·32

PDB, Protein Data Bank; ICT, isocitric acid; IK9, 1-[5-(cyclopropylsulfamoyl)-2-thiophen-3-yl-phenyl]-3-[3-(trifluoromethyl)phenyl]urea; NDO, nicotinamide-(6-deamino-6-hydroxy-adenine)-dinucleotide phosphate.
* To convert kcal to kJ, multiply it by 4·184.

Table 2. Summary of molecular docking experiments of naringenin and bacterial malate dehydrogenase

Target name	PDB code	Binding free energy (kcal/mol)*
Malate dehydrogenase CIT complexed	1EMD	−46·87
Malate dehydrogenase CIT complexed	2CMD	−40·31
Malate dehydrogenase NAD^+ complexed	1B8U	−30·45
Malate dehydrogenase NAD^+ complexed	1BMD	−31·03
Malate dehydrogenase NAD^+ complexed	1EMD	−47·19
Malate dehydrogenase NAD^+ complexed	1BDM	−29·11
Malate dehydrogenase NAD^+ complexed	1IE3	−43·14
Malate dehydrogenase NADPH complexed	1Y7T	−32·50
Malate dehydrogenase OAA complexed	1B8U	−30·92
Malate dehydrogenase PYR complexed	1IE3	−31·75

PDB, Protein Data Bank; CIT, citrate; OAA, oxaloacetate; PYR, pyruvic acid.
* To convert kcal to kJ, multiply it by 4·184.

Naringenin exhibited lower binding energy values when the interaction occurred on the cofactor binding sites of the bacterial enzymes IDH (NADP binding site) and MDH (NAD^+ complexed), with a calculated energy of −198·32 kJ/mol and −197·44 kJ/mol, respectively.

On Autodock4 molecular docking was possible to compare the energy of interaction of naringenin, L-malate, and NAD^+ with the human MDH in distinct conformations. Results are summarised in Table 3.

The interaction between human MDH and NAD^+ is much stronger than the interaction between MDH and naringenin and MDH and malate, suggesting naringenin is not able to compete straight with NAD^+ for the binding site. When structures 4WLN and 4WLV were employed for docking simulations, it was possible to observe that naringenin has the ability to bind on the L-malate site with lower energy (4WLN: −35·31 kJ /mol; 4WLV: −34·48 kJ/mol) than the L-malate itself (4WLN: −34·77 kJ/mol; 4WLV: −33·56 kJ/mol), suggesting that naringenin could replace L-malate molecule in the binding site prior to the binding of NAD^+ (Fig. 3).

Residue interaction

In order to study interactions at the molecular level between the bacterial IDH and MDH and naringenin, docking simulations were performed to describe the presence or absence of protein–ligand interactions and to understand how these interactions are established (hydrogen bonds, hydrophobic, etc.). Another concern was to know in which residues of the protein these interactions are identified.

The results of the docking simulation of bacterial IDH and MDH are shown in Tables 4 and 5, respectively. Referring to IDH and naringenin, four hydrogen bonds were demonstrated with the interacting residues of Lys82, Gly581, Ans85 and Arg145. It was also showed a hydrophobic interaction with Pro84. The distance between the interactions is between 2 and 4·6 Å.

Regarding MDH and naringenin, five hydrogen bonds were demonstrated with the interacting residues of Asp34, Cit313, Gly11, Arg80 and Asn11. It was also showed two hydrophobic

British Journal of Nutrition

Table 3. Summary of molecular docking experiments of naringenin, NAD^+ and L-malate on human malate dehydrogenase

Target name	PDB	Compound	Binding free energy (kcal/mol)*
Malate dehydrogenase	4WLN	L-Malate	−8·31
		Naringenin	−8·44
Malate dehydrogenase L-malate complexed	4WLF	L-Malate	−8·31
		Naringenin	−7·79
Malate dehydrogenase NAD^+ complexed	4WLV	NAD	−13·10
		L-Malate	−8·02
		Naringenin	−8·24
Malate dehydrogenase NAD^+ and L-malate complexed	4WLU	NAD	−10·86
		L-Malate	−8·54
		Naringenin	−8·26

PDB, Protein Data Bank.
* To convert kcal to kJ, multiply it by 4·184.

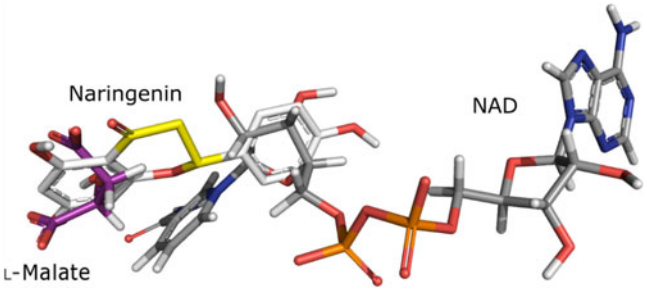

Fig. 3. Overlapping of L-malate (purple), NAD^+ (carbon atoms in grey) and naringenin (carbon atoms in white).

interactions with Arg80 and Ile12. The distance between the interactions is between 2 and 5 Å.

A model of the residue interaction is presented in Fig. 4.

Regarding human MDH, we found that naringenin can interact in the L-malate binding site (Fig. 5), at the Arg176, Pro99, Gly101, Val102, Ans142 and Gly234 residues. The L-malate interaction in the binding site also occurs through Arg176 and Gly234 residues, but does not share the remaining interaction found with the naringenin, connecting with Arg104, Arg110 and His200 (Fig. 6).

Discussion

Nowadays, society claims for healthier habits, including a massive antioxidant supplementation. However, the consumption of high levels of antioxidants, in fact, failed to bring the expected benefits, beyond stimulating carcinogen cell growth and even increasing the risk of cancer[16,26,57]. Herein, it was aimed to assess whether the naringenin supplementation during pregnancy could impact the mitochondrial metabolism in the cerebellum. Our results showed that naringenin intake during pregnancy produces adaptations in the TCA cycle in offspring's cerebellum, decreasing IDH, α-KGDH and MDH activities. Polyphenols as naringin (10, 20 and 40 mg/kg), morin (40 mg/kg) and epicatechin (20 mg/kg), at different periods of administration in adult rat (21–56 d), do not change TCA cycle enzymes activities in the heart[1,39,61,70]. However, banana flavonoids decreased MDH activity in male rat liver, administered at 0·1 mg/kg per d for 45 d[78].

To confirm the effect of naringenin on TCA enzymes, we assessed the *in vitro* effect of naringenin on commercially available purified dehydrogenases, in order to exclude tissue influences. We used a blood compatible concentration of naringenin in this study[49,72]. A significant reduction on α-KGDH (60 %) and MDH (70 %) was observed, which is comparable to the results obtained in the cerebellum of pups submitted to maternal naringenin administration. Considering that naringenin supplementation during pregnancy reduced specifically the dehydrogenases from TCA cycle, and it was recently found that polyphenols might compete with nicotinamide derivatives by the enzyme site binding[37], we hypothesised that naringenin can surpass the placental barrier[2,13,56,66] and bind specifically in NAD^+ site, inhibiting the TCA cycle dehydrogenases.

To clarify this idea, we tested bacterial and human TCA cycle enzymes on different docking models to evaluate if naringenin could really interact with the protein structures, and the results are strongly correlated with the *in vitro* and *in vivo* naringenin effect. We show that both in bacterial and human enzymes, naringenin was able to bind at different enzyme sites, being the binding with the bacterial IDH and MDH most probable at the site of the cofactor NAD^+. In the human MDH, the binding seems to occupy the malate site more strongly than the substrate itself in the apo state, being able to prevent or delay the enzymatic reaction. When docking was realised in other states of the enzyme, naringenin also shows binding potential. Binding free-energy values are known to provide an important idea of the affinity in the interaction of proteins to diverse compounds, being well used in the discovery of new drugs[9,15].

The most part of bacterial enzymes interactions have occurred by means of hydrogen bonds and hydrophobic interactions, which make a large contribution to protein–ligand stability[25,80], and present maximum 5 Å distance. In human MDH, the interaction with the enzyme at the malate site has

Table 4. Summary of ligand interactions of naringenin and isocitrate dehydrogenase

Receptor–ligand interactions	Distance	Category	Type	From		To	
NAR:H10–LYS82:O	265 187	Hydrogen bond	Conventional	NAR:H10	H-donor	LYS82:O	H-acceptor
NAR:H11–GLY581:O	200 664	Hydrogen bond	Conventional	NAR:H11	H-donor	GLY581:O	H-acceptor
LYS82:HZ3–NAR:O3	207 511	Hydrogen bond	Conventional	LYS82:HZ3	H-donor	NAR:O3	H-acceptor
ASN85:H–NAR:O2	278 133	Hydrogen bond	Conventional	ASN85:H	H-donor	NAR:O2	H-acceptor
ARG145:HH21–NAR:O4	243 983	Hydrogen bond	Conventional	ARG145:HH21	H-donor	NAR:O4	H-acceptor
NAR–PRO84	457 527	Hydrophobic	Pi-alkyl	NAR	Pi-orbitals	PRO84	Alkyl

Table 5. Summary of ligand interactions of naringenin and malate dehydrogenase

Receptor–ligand interactions	Distance	Category	Type	From		To	
NAR:H10–ASP34:OD2	211 226	Hydrogen bond	Conventional	NAR:H10	H-donor	ASP34:OD2	H-acceptor
NAR:H12–CIT313:O3	201 006	Hydrogen bond	Conventional	NAR:H12	H-donor	CIT313:O3	H-acceptor
GLY11:H–NAR:O1	200 139	Hydrogen bond	Conventional	GLY11:H	H-donor	NAR:O1	H-acceptor
ARG80:HE–NAR:O1	260 711	Hydrogen bond	Conventional	ARG80:HE	H-donor	NAR:O1	H-acceptor
ARG80:HH22–NAR:O1	29 779	Hydrogen bond	Conventional	ARG80:HH22	H-donor	NAR:O1	H-acceptor
ASN119:H–NAR:O5	232 456	Hydrogen bond	Conventional	ASN119:H	H-donor	NAR:O5	H-acceptor
CIT313:O4–NAR	417 451	Hydrogen bond	Pi-donor	CIT313:O4	H-donor	NAR	Pi-orbitals
NAR–ILE12	50 004	Hydrophobic	Pi-alkyl	NAR	Pi-orbitals	ILE12	Alkyl
NAR–ARG80	50 221	Hydrophobic	Pi-alkyl	NAR	Pi-orbitals	ARG80	Alkyl

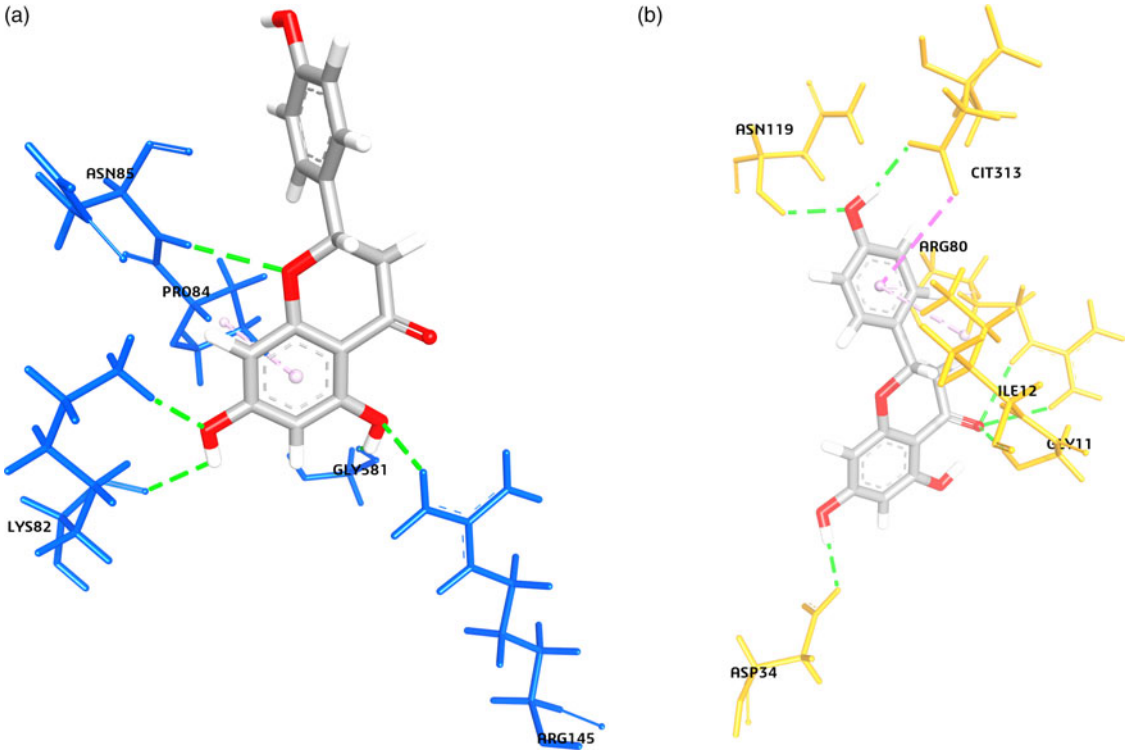

Fig. 4. Isocitrate dehydrogenase (a) and malate dehydrogenase (b). Potential hydrogen bonds are dotted in green, and π-interactions are dotted in pink. Residues are shown as sticks and coloured orange. Naringenin is present as sticks in grey colour, oxygens are in red and hydrogens in white.

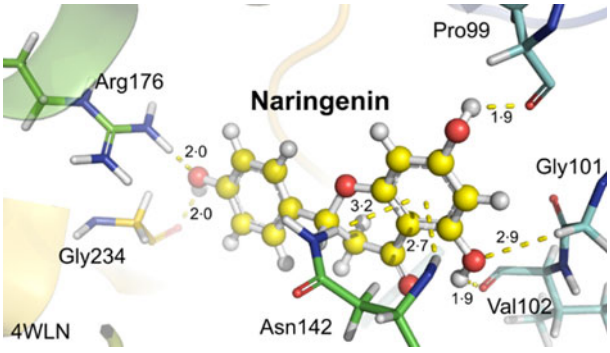

Fig. 5. Network of naringenin interactions at the L-malate binding site. Data obtained from the docking of naringenin in the malate dehydrogenase (MDH) apo structure (4WLN). Naringenin is shown in ball and sticks representation, and main interactions are depicted as yellow dashes. The distance between atoms was measured in Å.

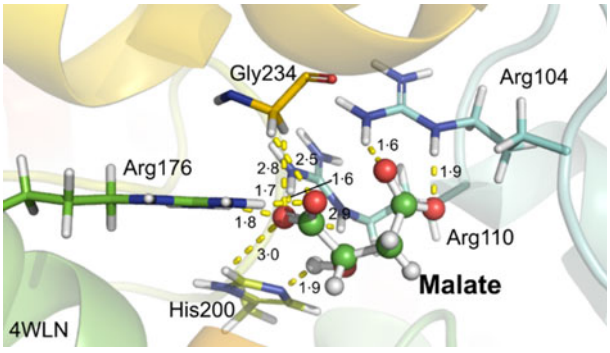

Fig. 6. Detailed representation of L-malate interactions network in the binding site of malate dehydrogenase (MDH). Data obtained from docking using the MDH apo structure (4WLN). L-Malate is shown in ball and sticks representation, and main interactions are depicted as yellow dashes. The distance between atoms was measured in Å.

British Journal of Nutrition

demonstrated to share two residues in relation to the substrate bound and this reaction is more favourable to naringenin than to malate, presenting 1·9–3·2 Å distance between interactions.

Taking into account that naringenin could interact with the TCA enzymes prior to the substrate, we have shown that naringenin inhibits the TCA dehydrogenases and may affect the brain mitochondrial energy metabolism, as demonstrated in the *in vivo, in vitro* and *in silico* experiments. A recent study has shown that a diet rich in polyphenols in the third trimester of pregnancy cause fetal ductal constriction[89], and the effect identified is further evidence that high consumption of polyphenols during pregnancy may bring negative adaptations to the fetus.

Conclusion

Maternal diet could affect brain metabolic programming of the fetus. We have demonstrated that naringenin supplementation during pregnancy inhibits TCA cycle dehydrogenases in the cerebellum of rat pups. *In vitro* experiments confirmed that naringenin reduces TCA cycle dehydrogenases activities, probably acting directly on substrate and cofactor site as demonstrated by the molecular docking approach. Our findings suggest that polyphenols supplementation during pregnancy should be carefully evaluated, considering the interference in essential enzymes for energy metabolism, jeopardising brain development.

Acknowledgements

This work was supported by Conselho Nacional de Desenvolvimento Científico e Tecnológico (CNPq – Universal 442406/2014-2 and INCT 465671/2014-4), and Pró-Reitoria de Pesquisa/Universidade Federal do Rio Grande do Sul (PROPESQ/UFRGS).

All authors had substantial involvement in the study design, data acquisition, analysis and interpretation. In addition, all authors read and approved the final document.

The authors declare that they have no conflicts of interest.

References

1. Al Numair KS, Chandramohan G, Alsaif MA, *et al.* (2012) Protective effect of morin on cardiac mitochondrial function during isoproterenol-induced myocardial infarction in male Wistar rats. *Redox Rep* **17**, 14–21.
2. Arola-Arnal A, Oms-Oliu G, Crescenti A, *et al.* (2013) Distribution of grape seed flavanols and their metabolites in pregnant rats and their fetuses. *Mol Nutr Food Res* **57**, 1741–1752.
3. August PM, Maurmann RM, Saccomori AB, *et al.* (2018) Effect of maternal antioxidant supplementation and/or exercise practice during pregnancy on postnatal overnutrition induced by litter size reduction: brain redox homeostasis at weaning. *Int J Dev Neurosci* **71**, 146–155.
4. Barker DJ (1990) The fetal and infant origins of adult disease. *BMJ* **301**, 1111.
5. Barker DJ, Winter PD, Osmond C, *et al.* (1989) Weight in infancy and death from ischaemic heart disease. *Lancet* **ii**, 577–580.
6. Bell JK, Yennawar HP, Wright SK, *et al.* (2001) Structural analyses of a malate dehydrogenase with a variable active site. *J Biol Chem* **276**, 31156–31162.
7. Berman HM, Westbrook J, Feng Z, *et al.* (2000) The protein data bank. *Nucleic Acids Res* **28**, 235–242.
8. Bernatoniene J, Kopustinskiene DM, Jakstas V, *et al.* (2014) The effect of *Leonurus cardiaca* herb extract and some of its flavonoids on mitochondrial oxidative phosphorylation in the heart. *Planta Med* **80**, 525–532.
9. Broomhead NK & Soliman ME (2017) Can we rely on computational predictions to correctly identify ligand binding sites on novel protein drug targets? Assessment of binding site prediction methods and a protocol for validation of predicted binding sites. *Cell Biochem Biophys* **75**, 15–23.
10. Callegari-Jacques SM (2003) *Bioestatística: Princípios e aplicações (Biostatistics: Principles and Applications)*. Porto Alegre: Artmed.
11. Campos-Acevedo AA, Garcia-Orozco KD, Sotelo-Mundo RR, *et al.* (2013) Expression, purification, crystallization and X-ray crystallographic studies of different redox states of the active site of thioredoxin 1 from the whiteleg shrimp *Litopenaeus vannamei*. *Acta Crystallogr Sect F Struct Biol Cryst Commun* **69**, 488–493.
12. Canetta S, Sourander A, Surcel HM, *et al.* (2014) Elevated maternal C-reactive protein and increased risk of schizophrenia in a national birth cohort. *Am J Psychiatry* **171**, 960–968.
13. Cao L, Pu J, Cao QR, *et al.* (2013) Pharmacokinetics of puerarin in pregnant rats at different stages of gestation after oral administration. *Fitoterapia* **86**, 202–207.
14. Cherbavaz DB, Lee ME, Stroud RM, *et al.* (2000) Active site water molecules revealed in the 21 A resolution structure of a site-directed mutant of isocitrate dehydrogenase. *J Mol Biol* **295**, 377–385.
15. Christ CD & Fox T (2014) Accuracy assessment and automation of free energy calculations for drug design. *J Chem Inf Model* **54**, 108–120.
16. DeNicola GM, Karreth FA, Humpton TJ, *et al.* (2011) Oncogene-induced Nrf2 transcription promotes ROS detoxification and tumorigenesis. *Nature* **475**, 106–109.
17. Dolinsky TJ, Czodrowski P, Li H, *et al.* (2007) PDB2PQR: expanding and upgrading automated preparation of biomolecular structures for molecular simulations. *Nucleic Acids Res* **35**, W522–W525.
18. Dolinsky TJ, Nielsen JE, McCammon JA, *et al.* (2004) PDB2PQR: an automated pipeline for the setup of Poisson-Boltzmann electrostatics calculations. *Nucleic Acids Res* **32**, W665–667.
19. Eo, YM, Han BG & HC Ahn (2015) Crystal structure of apo MDH2. Protein Data Bank.
20. Eo, YM, Han BG & HC Ahn (2015) Crystal structure of L-malate and NAD bound MDH2.
21. Eo, YM, Han BG & HC Ahn (2015) Crystal structure of L-malate bound MDH2.
22. Eo, YM, Han BG & HC Ahn (2015) Crystal structure of NAD bound MDH2. Protein Data Base.
23. Fernandez-Twinn DS, Hjort L, Novakovic B, *et al.* (2019) Intrauterine programming of obesity and type 2 diabetes. *Diabetologia* **62**, 1789–1801.
24. Fernandez-Twinn DS & Ozanne SE (2010) Early life nutrition and metabolic programming. *Ann N Y Acad Sci* **1212**, 78–96.
25. Gholami S & Bordbar AK (2014) Exploring binding properties of naringenin with bovine beta-lactoglobulin: a fluorescence, molecular docking and molecular dynamics simulation study. *Biophys Chem* **187–188**, 33–42.
26. Ginter E, Simko V & Panakova V (2014) Antioxidants in health and disease. *Bratisl Lek Listy* **115**, 603–606.
27. Goncalves S, Miller SP, Carrondo MA, *et al.* (2012) Induced fit and the catalytic mechanism of isocitrate dehydrogenase. *Biochemistry* **51**, 7098–7115.

28. Hahn M, Baierle M, Charao MF, *et al.* (2017) Polyphenol-rich food general and on pregnancy effects: a review. *Drug Chem Toxicol* **40**, 368–374.
29. Hales CN & Barker DJ (1992) Type 2 (non-insulin-dependent) diabetes mellitus: the thrifty phenotype hypothesis. *Diabetologia* **35**, 595–601.
30. Hall MD & Banaszak LJ (1993) Crystal structure of a ternary complex of *Escherichia coli* malate dehydrogenase citrate and NAD at 1·9 Å resolution. *J Mol Biol* **232**, 213–222.
31. Hall MD, Levitt DG & Banaszak LJ (1992) Crystal structure of *Escherichia coli* malate dehydrogenase A complex of the apoenzyme and citrate at 187 A resolution. *J Mol Biol* **226**, 867–882.
32. Halperin I, Ma B, Wolfson H, *et al.* (2002) Principles of docking: an overview of search algorithms and a guide to scoring functions. *Proteins* **47**, 409–443.
33. Huang LS, Sun G, Cobessi D, *et al.* (2006) 3-Nitropropionic acid is a suicide inhibitor of mitochondrial respiration that, upon oxidation by complex II, forms a covalent adduct with a catalytic base arginine in the active site of the enzyme. *J Biol Chem* **281**, 5965–5972.
34. Huey R, Morris GM, Olson AJ, *et al.* (2007) A semiempirical free energy force field with charge-based desolvation. *J Comput Chem* **28**, 1145–1152.
35. Inaoka DK, Shiba T, Sato D, *et al.* (2015) Structural insights into the molecular design of Flutolanil derivatives targeted for Fumarate respiration of parasite mitochondria. *Int J Mol Sci* **16**, 15287–15308.
36. Irwin JJ & Shoichet BK (2005) ZINC–a free database of commercially available compounds for virtual screening. *J Chem Inf Model* **45**, 177–182.
37. Islam B, Sharma C, Adem A, *et al.* (2015) Insight into the mechanism of polyphenols on the activity of HMGR by molecular docking. *Drug Des Devel Ther* **9**, 4943–4951.
38. Iwashina T (2015) Contribution to flower colors of flavonoids including anthocyanins: a review. *Nat Prod Commun* **10**, 529–544.
39. Jayachandran KS, Vasanthi HR & Rajamanickama GV (2010) Flavonoid rich fraction of *Dioscorea bulbifera* Linn (Yam) enhances mitochondrial enzymes and antioxidant status and thereby protects heart from isoproterenol induced myocardial infarction. *Curr Pharm Biotechnol* **11**, 887–894.
40. Kelly CA, Nishiyama M, Ohnishi Y, *et al.* (1993) Determinants of protein thermostability observed in the 19-A crystal structure of malate dehydrogenase from the thermophilic bacterium *Thermus flavus*. *Biochemistry* **32**, 3913–3922.
41. Khan MB, Khan MM, Khan A, *et al.* (2012) Naringenin ameliorates Alzheimer's disease (AD)-type neurodegeneration with cognitive impairment (AD-TNDCI) caused by the intracerebroventricular-streptozotocin in rat model. *Neurochem Int* **61**, 1081–1093.
42. Kim CS, Kwon Y, Choe SY, *et al.* (2015) Quercetin reduces obesity-induced hepatosteatosis by enhancing mitochondrial oxidative metabolism via heme oxygenase-1. *Nutr Metab (Lond)* **12**, 33.
43. Kim SY, Hwang KY, Kim SH, *et al.* (1999) Structural basis for cold adaptation Sequence, biochemical properties, and crystal structure of malate dehydrogenase from a psychrophile *Aquaspirillum arcticum*. *J Biol Chem* **274**, 11761–11767.
44. Kim Y, Keogh JB & Clifton PM (2016) Polyphenols and glycemic control. *Nutrients* **8**, E17.
45. Kitto GB (1969) Intra- and extramitochondrial malate dehydrogenases from chicken and tuna heart. *Methods Enzymol* **13**, 106–116.
46. Lai JC & Cooper AJ (1986) Brain alpha-ketoglutarate dehydrogenase complex: kinetic properties, regional distribution, and effects of inhibitors. *J Neurochem* **47**, 1376–1386.
47. Lewicka A, Szymański Ł, Rusiecka K, *et al.* (2019) Supplementation of plants with immunomodulatory properties during pregnancy and lactation-maternal and offspring health effects. *Nutrients* **11**, E1958.
48. Lowry OH, Rosebrough NJ, Farr AL, *et al.* (1951) Protein measurement with the Folin phenol reagent. *J Biol Chem* **193**, 265–275.
49. Mata-Bilbao Mde L, Andres-Lacueva C, Roura E, *et al.* (2007) Absorption and pharmacokinetics of grapefruit flavanones in beagles. *Br J Nutr* **98**, 86–92.
50. Mesecar AD, Stoddard BL & Koshland DE (1997) Orbital steering in the catalytic power of enzymes: small structural changes with large catalytic consequences. *Jr Science* **277**, 202–206.
51. Mohammad MK, Al-Masri IM, Taha MO, *et al.* (2008) Olanzapine inhibits glycogen synthase kinase-3beta: an investigation by docking simulation and experimental validation. *Eur J Pharmacol* **584**, 185–191.
52. Morris GM, Goodsell DS, Halliday RS, *et al.* (1998) Automated docking using a Lamarckian genetic algorithm and an empirical binding free energy function. *J Comput Chem* **19**, 1639–1662.
53. Morris GM, Huey R, Lindstrom W, *et al.* (2009) AutoDock4 and AutoDockTools4: automated docking with selective receptor flexibility. *J Comput Chem* **30**, 2785–2791.
54. Murphy SK, Fineberg AM, Maxwell SD, *et al.* (2017) Maternal infection and stress during pregnancy and depressive symptoms in adolescent offspring. *Psychiatry Res* **257**, 102–110.
55. Myburgh KH (2014) Polyphenol supplementation: benefits for exercise performance or oxidative stress? *Sports Med* **44**, S57–70.
56. Nigam SK, Bush KT, Martovetsky G, *et al.* (2015) The organic anion transporter (OAT) family: a systems biology perspective. *Physiol Rev* **95**, 83–123.
57. Omenn GS, Goodman GE, Thornquist MD, *et al.* (1996) Effects of a combination of beta carotene and vitamin A on lung cancer and cardiovascular disease. *N Engl J Med* **334**, 1150–1155.
58. Peng Y, Zhong C, Huang W, *et al.* (2008) Structural studies of *Saccharomyces cerevisiae* mitochondrial NADP-dependent isocitrate dehydrogenase in different enzymatic states reveal substantial conformational changes during the catalytic reaction. *Protein Sci* **17**, 1542–1554.
59. Plaut GW (1969) Isocitrate dehydrogenase from bovine heart. *Methods Enzymol* **13**, 34–42.
60. Ponzo V, Goitre I, Fadda M, *et al.* (2015) Dietary flavonoid intake and cardiovascular risk: a population-based cohort study. *J Transl Med* **13**, 218.
61. Rajadurai M & Prince PS (2007) Preventive effect of naringin on cardiac mitochondrial enzymes during isoproterenol-induced myocardial infarction in rats: a transmission electron microscopic study. *J Biochem Mol Toxicol* **21**, 354–361.
62. Raza SS, Khan MM, Ahmad A, *et al.* (2013) Neuroprotective effect of naringenin is mediated through suppression of NF-kappaB signaling pathway in experimental stroke. *Neuroscience* **230**, 157–171.
63. Rosenthal RE, Hamud F, Fiskum G, *et al.* (1987) Cerebral ischemia and reperfusion: prevention of brain mitochondrial injury by lidoflazine. *J Cereb Blood Flow Metab* **7**, 752–758.
64. Sabarinathan D, Mahalakshmi P & Vanisree AJ (2011) Naringenin, a flavanone inhibits the proliferation of cerebrally implanted C6 glioma cells in rats. *Chem Biol Interact* **189**, 26–36.
65. Sanner MF (1999) Python: a programming language for software integration and development. *J Mol Graph Model* **17**, 57–61.
66. Schroder-van der Elst JP, van der Heide D, Rokos H, *et al.* (1998) Synthetic flavonoids cross the placenta in the rat and are found in fetal brain. *Am J Physiol* **274**, E253–E256.

British Journal of Nutrition

67. Schrödinger L (2010) The PyMOL Molecular Graphics System, Version 1.3.
68. Sidhu NS, Delbaere LT & Sheldrick GM (2011) Structure of a highly $NADP^+$-specific isocitrate dehydrogenase. *Acta Crystallogr D Biol Crystallogr* **67**, 856–869.
69. Srere PA (1969) Citrate synthase: [EC 4.1.3.7. Citrate oxaloacetate-lyase (CoA-acetylating)]. *Methods Enzymol* **13**, 3–11.
70. Stanely Mainzen Prince P (2013) (-) Epicatechin attenuates mitochondrial damage by enhancing mitochondrial multi-marker enzymes, adenosine triphosphate and lowering calcium in isoproterenol induced myocardial infarcted rats. *Food Chem Toxicol* **53**, 409–416.
71. Sun F, Huo X, Zhai Y, *et al.* (2005) Crystal structure of mitochondrial respiratory membrane protein complex II. *Cell* **121**, 1043–1057.
72. Sun Z, Zhao L, Zuo L, *et al.* (2014) A UHPLC-MS/MS method for simultaneous determination of six flavonoids, gallic acid and 5,8-dihydroxy-1,4-naphthoquinone in rat plasma and its application to a pharmacokinetic study of Cortex Juglandis Mandshuricae extract. *J Chromatogr B Analyt Technol Biomed Life Sci* **958**, 55–62.
73. Taegtmeyer H, Sen S & Vela D (2010) Return to the fetal gene program: a suggested metabolic link to gene expression in the heart. *Ann N Y Acad Sci* **1188**, 191–198.
74. Tomita T, Fushinobu S, Kuzuyama T, *et al.* (2005) Crystal structure of NAD-dependent malate dehydrogenase complexed with NADP(H). *Biochem Biophys Res Commun* **334**, 613–618.
75. Toumi ML, Merzoug S, Baudin B, *et al.* (2013) Quercetin alleviates predator stress-induced anxiety-like and brain oxidative signs in pregnant rats and immune count disturbance in their offspring. *Pharmacol Biochem Behav* **107**, 1–10.
76. Tretter L & Adam-Vizi V (2004) Generation of reactive oxygen species in the reaction catalyzed by alpha-ketoglutarate dehydrogenase. *J Neurosci* **24**, 7771–7778.
77. Vanhees K, van Schooten FJ, van Waalwijk van Doorn-Khosrovani SB, *et al.* (2013) Intrauterine exposure to flavonoids modifies antioxidant status at adulthood and decreases oxidative stress-induced DNA damage. *Free Radic Biol Med* **57**, 154–161.
78. Vijayakumar S, Presannakumar G & Vijayalakshmi NR (2009) Investigations on the effect of flavonoids from banana, Musa paradisiaca L on lipid metabolism in rats. *J Diet Suppl* **6**, 111–123.
79. Wang J, Yang Z, Lin L, *et al.* (2012) Protective effect of naringenin against lead-induced oxidative stress in rats. *Biol Trace Elem Res* **146**, 354–359.
80. Weng C, Fu Y, Jiang H, *et al.* (2015) Binding interaction between a queen pheromone component HOB and pheromone binding protein ASP1 of Apis cerana. *Int J Biol Macromol* **72**, 430–436.
81. Xiang AH, Wang X, Martinez MP, *et al.* (2015) Association of maternal diabetes with autism in offspring. *JAMA* **313**, 1425–1434.
82. Yamada T, Hayasaka S, Shibata Y, *et al.* (2011) Frequency of citrus fruit intake is associated with the incidence of cardiovascular disease: the Jichi Medical School Cohort study. *J Epidemiol* **21**, 169–175.
83. Yang X, Yang J, Xu C, *et al.* (2015) Antidiabetic effects of flavonoids from Sophora flavescens EtOAc extract in type 2 diabetic KK-ay mice. *J Ethnopharmacol* **171**, 161–170.
84. Yankovskaya V, Horsefield R, Tornroth S, *et al.* (2003) Architecture of succinate dehydrogenase and reactive oxygen species generation. *Science* **299**, 700–704.
85. Yasutake Y, Watanabe S, Yao M, *et al.* (2002) Structure of the monomeric isocitrate dehydrogenase: evidence of a protein monomerization by a domain duplication. *Structure* **10**, 1637–1648.
86. Yasutake Y, Watanabe S, Yao M, *et al.* (2003) Crystal structure of the monomeric isocitrate dehydrogenase in the presence of $NADP^+$: insight into the cofactor recognition, catalysis, and evolution. *J Biol Chem* **278**, 36897–36904.
87. Zielinsky P & Busato S (2013) Prenatal effects of maternal consumption of polyphenol-rich foods in late pregnancy upon fetal ductus arteriosus. *Birth Defects Res C Embryo Today* **99**, 256–274.
88. Zielinsky P, Martignoni FV & Vian I (2014) Deleterious effects of maternal ingestion of cocoa upon fetal ductus arteriosus in late pregnancy. *Front Pharmacol* **5**, 281.
89. Zielinsky P, Piccoli AL, Manica JL, *et al.* (2010) New insights on fetal ductal constriction: role of maternal ingestion of polyphenol-rich foods. *Expert Rev Cardiovasc Ther* **8**, 291–298.
90. Zielinsky P, Piccoli AL, Vian I, *et al.* (2013) Maternal restriction of polyphenols and fetal ductal dynamics in normal pregnancy: an open clinical trial. *Arq Bras Cardiol* **101**, 217–225.

British Journal of Nutrition